

# ANALYTICAL SOLUTIONS IN THE MODELING OF THE ENDOVENOUS LASER ABLATION

LUISA CONSIGLIERI

**ABSTRACT.** We model the operative treatment of incompetent truncal veins using endovenous laser ablation (EVLA). Three differential equations, namely the diffusion, the heat and the bioheat equations, are considered in the endovenous-perivenous multidomain, describing the lumen, the vein wall, the tissue pad and the skin. Exact solutions are provided. Our main concern is to accurately model the heat source by taking the Beer–Lambert law into account in the irradiance of the incident beam. To accurately model the heat transfer at the skin boundary, the Newton law of cooling is considered as a Robin boundary condition. Open problems are presented.

## 1. INTRODUCTION

Conventional high ligation and stripping (crosssection of the saphenofemoral junction (SFJ) with great saphenous vein (GSV) stripping) and radio-frequency (RF) ablation therapies are passing their legacy to the new technologies such as the laser (and the ultrasound-guided foam sclerotherapy) in the treatment of varicose veins [6, 13, 34, 41]. Also the extremely high degree of recurrence occurring after previous ligation and stripping of the great saphenous vein ask for the safety and efficacy of endovenous laser ablation as a posterior treatment for recurrent symptomatic saphenous insufficiency [2]. In the recent years, several clinical follow-up studies (see, for instance, [12, 15, 16, 23, 25, 33]) have reported different laser systems to treat incompetent GSV. Indeed, the advantages of the endovenous laser surgery are more relevant than its complications [3]. Clinical studies address failure as patency or recanalization of the GSV or residual symptoms [14], the occlusion, ulcer healing, paresthesia rates and postoperative pain [28, 35], as other adverse side effects [37, 39]. Although it is unknown its cause even an ischemic stroke following endovenous laser treatment of varicose veins is reported [5].

The fiber type is the single most significant factor related to treatment outcome [31]. For effective endovenous laser (EVL) therapy, the laser wavelength varies from  $\lambda = 810$  nm [37, 41] until to 980 nm [38], at power settings of 9 W to 17 W [35] according to the diameter and severity of varicose veins. The 1470-nm wavelength EVL system successfully closes saphenous veins but not acts as "anesthesia-less thermal ablation technology" [1]. In [32], the authors found that after EVLA with low-energy density, worse results and more relapses could be expected than with higher-energy doses.

---

2020 *Mathematics Subject Classification.* Primary: 92C50; Secondary: 35A24.

*Key words and phrases.* EVLA; fluence rate; Beer–Lambert law; Newton law of cooling; Bioheat transfer equation; thermal damage; exact solutions.

A vast literature has been playing a prominent and broad-spectrum role in the study of the temperature dependence of the thermophysical and mechanical properties of biological tissues (see [4] and the references therein). The aim of some studies is to determine how the heat sink effect of the blood flow inside the vessel may either be measured [8, 11, 20], distort coagulation volume during thermal therapies [19, 43], or protect the vessel wall in the proximity of an RF-assisted resection device [17]. In this last work, the tissue vaporization was modeled by the enthalpy method, while parametric studies were conducted in [8] to prove the blood flow has a cooling effect during RF ablation treatment. The present goal goes somewhat on the opposite direction: to study how the laser wavelength behaves and the damage of blood vessels is influenced.

The finding of mathematical models is essential to control the temperature, and to prevent postoperative complications. It includes handling of mathematical problems generated by the application of models to real thermal conditions. The combination Mordon's optical-thermal model with the presence of a strongly absorbing carbonized blood layer on the fiber tip is introduced in [42] by neglecting the Arrhenius damage integral, and after is developed in [29]. We refer to [21] a finite element modeling of the influence of air cooling that simulates the perisaphenous subcutaneous tumescent saline solution infiltration. Some analytical solutions to the bioheat transfer problem are studied in multiregion [9, 10], where the Joule effect is assumed to be constant.

Here, we follow the whole path from the phenomenological interpretation of thermal therapy to scientific computing for producing simulations. Bearing this in mind, one mathematical model is stated and analytically solved such that the final method will be very fast to execute. To validate our model, we compare our results with experimental measurements.

## 2. MATHEMATICAL MODEL

The optical laser fiber is inserted into the sheath so that the fiber tip extends 2 cm beyond the end of the sheath to avoid the melting of the sheath material [37, 38]. The geometry of the fiber-tissue system is assumed to be as follows (cf. Fig. 1). The fiber probe (with radius  $r_f$ ) is assumed to be centered in the middle of the vein, where the vein segment  $\Omega_v = \Omega_{\text{lumen}} \cup \Omega_w$  is assumed to be cylindrical with  $r_i$  and  $\varepsilon$  being the inner radius and the thickness of the venous wall, respectively. In vivo, the thickness of the venous wall is approximately one tenth the width of its blood column:  $\varepsilon = r_i/5$ .

The saphenous vein is considered to be parallel to the skin surface [21]. Then the complete domain  $\Omega = \Omega_v \cup \Omega_{\text{pad}} \cup \Omega_{\text{skin}}$  is assumed to be constituted by axially half-cylindrical volumes, namely vein, perivenous and skin tissues. The tissue around the venous may be considered homogenous. The thickness of the perivenous and skin tissues are  $l_{\text{pad}} = 10$  mm and  $l_{\text{skin}} = 3$  mm, respectively.

The procedure begins by inserting the laser sheath and positioning the bare tip below SFJ. At time  $t = 0$ , the fiber tip is located at axial coordinate  $z_0$ . The fiber is kept in a piecewise pull-back model until the level of the knee. A pulling back of the laser fiber and the introduced catheter is at a constant velocity  $v$ , when the irradiation is activated, and then they may be pulled back by increments, during the off periods.

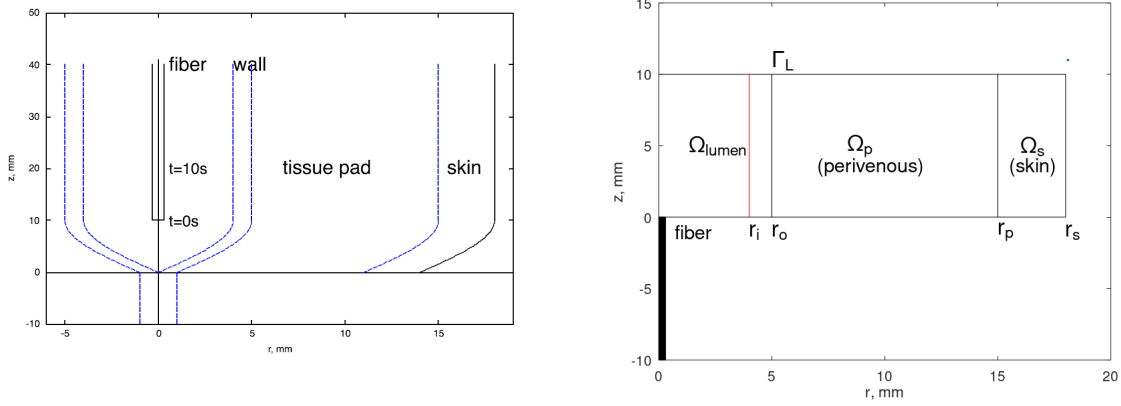


FIGURE 1. Left: Schematic sagittal representation of the endovenous fiber at the initial instant of time  $t = 0$ . Right: Schematic cylindrical representations in 2D of the lumen  $\Omega_{\text{lumen}} = \{(x, y) : x^2 + y^2 < r_i^2\} \times ]0; L[$ , the wall  $\Omega_w = \{(x, y) : r_i^2 < x^2 + y^2 < (r_i + \varepsilon)^2\} \times ]0; L[$ , the tissue pad  $\Omega_{\text{pad}} = \{(x, y) : (r_i + \varepsilon)^2 < x^2 + y^2 < r_p^2\} \times ]0; L[$ , and the skin  $\Omega_{\text{skin}} = \{(x, y) : r_p^2 < x^2 + y^2 < r_s^2\} \times ]0; L[$ .

The cycle is repeated until a desired fixed distance. This piecewise pull-back in the application of laser light is preferred because the manually made continuous pull-back depends on the operating surgeon technique and experience. For each fixed irradiation time  $t_{\text{end}} > 0$ ,  $L > 0$  stands for the corresponding length of the treated vein segment.

We assume that outer surface  $\Gamma_L = \{(x, y) : x^2 + y^2 < r_s^2\} \times \{L\}$  is an insulating boundary, that is, there is no outflow.

**2.1. Diffusion approximation of the radiative transfer equation.** The light power emitted out of the fiber tip into the ambient blood is scattered towards the vein wall and the surrounding tissue. The fluence rate  $\phi$  [ $\text{W m}^{-2}$ ] verifies the diffusion equation (see, for instance, [40])

$$\frac{1}{\nu} \frac{\partial \phi}{\partial t} - D \Delta \phi + \mu_a \phi = S \quad \text{in } \Omega \times ]0; t_{\text{end}}[, \quad (1)$$

where:

$\nu = c/n$ : is the speed of light in the tissue [ $\text{m s}^{-1}$ ], as determined by the relative refractive index  $n$ ;

$D = \frac{1}{3(\mu_a + \mu'_s)}$ : is the diffusion coefficient;

$\mu_a$ : is the absorption coefficient [ $\text{m}^{-1}$ ];

$\mu'_s = (1 - g)\mu_s$ : is the reduced scattering coefficient [ $\text{m}^{-1}$ ], with  $g$  being the scattering anisotropy coefficient, and  $\mu_s$  being the scattering coefficient;

$S$ : is the source of scattered photons [ $\text{W m}^{-3}$ ], which represents the power injected in the unit volume.

Usually  $S$  is assumed to be a source point in order to use the Green functions in the determination of the solution  $\phi$  of the diffusion equation (1). For a single spherically symmetric point source emitting  $P_{\text{laser}}$  [W], the form of  $\phi$  at a distance  $r$  from the source is  $P_{\text{laser}} \exp(-\mu_{\text{eff}}r)/(4\pi Dr)$  [24], where  $\mu_{\text{eff}} = \sqrt{3\mu_a(\mu_a + \mu'_s)}$  represents the effective attenuation coefficient.

Laser energy is delivered along the vein with a continuous emission [2], and a fiber pull-back is kept at about 1-cm increment every 10 seconds [3]. In this work, we consider

$$S(r, z, t) \equiv S(r_{\text{f}}, z, t) = \frac{P_{\text{laser}}}{\pi r_{\text{f}}^2} \frac{\mu_s(\mu_t + g\mu_a)}{\mu_a + \mu'_s} \exp[-\mu_t(z + vt)], \quad (2)$$

for all  $(r, z, t) \in [0; r_{\text{f}}[\times] - vt; L[\times[0; t_{\text{end}}[$ , where  $\mu_t = \mu_a + \mu_s$  is the attenuation coefficient *i.e.* the reciprocal of the average distance light travels before being scattered or absorbed by the medium. The above expression stands for the Beer–Lambert law [30] when  $t = 0$ , while stands for the velocity of the fiber pull-back with increment  $L = 10$  mm and time  $t_{\text{end}} = 10$  s, *i.e.* at a velocity  $v = 1.0$  mm s<sup>-1</sup>.

**2.2. Heat transfer.** The heat energy was delivered directly to the vein wall [37], due to that the compression reduces the vein diameter. Heat transfer due to the energy of light deposited is described by the following heat and bioheat transfer equations:

$$\rho c_p \left( \frac{\partial T}{\partial t} + \mathbf{u} \cdot \nabla T \right) = \nabla \cdot (k \nabla T) + q \quad \text{in } \Omega_{\text{lumen}} \times ]0; t_{\text{end}}[; \quad (3)$$

$$\rho c_p \frac{\partial T}{\partial t} + c_b \omega (T - T_b) = \nabla \cdot (k \nabla T) + q \quad \text{in } (\Omega_w \cup \Omega_p \cup \Omega_s) \times ]0; t_{\text{end}}[, \quad (4)$$

where:

- $T$ : is the temperature [K];
- $\mathbf{u}$ : is the blood velocity vector [m s<sup>-1</sup>];
- $\rho$ : is the density [kg m<sup>-3</sup>];
- $c_p$ : is the specific heat capacity per unit mass [J kg<sup>-1</sup> K<sup>-1</sup>];
- $k$ : is the thermal conductivity [W m<sup>-1</sup> K<sup>-1</sup>];
- $q$ : is the heat source caused by laser power [W m<sup>-3</sup>].

Considering laminar flow, the blood velocity is scalar, and the convective term in (3) reads  $u \frac{\partial T}{\partial z}$ . In the heat equation (3),  $\rho = \rho_b$  and  $c_p = c_b$  denote the density and the specific heat capacity of the blood, respectively. The Pennes bioheat transfer equation (4), which distinguishes itself from nonliving systems, includes the effects of blood perfusion  $\omega = \rho_b w$  [kg m<sup>-3</sup> s<sup>-1</sup>] that occurs in the capillary bed, that is, the energy transfer term  $-c_b \omega (T - T_b)$  is consequence of the mass transport of blood through tissue (cf. Table 1). Here,  $T_b$  represents the temperature of the blood (assumed to be 38 °C),  $w$  denotes the volumetric flow [s<sup>-1</sup>], and  $c_b \omega$  accounts for the heat conducted in direction of the contribution of flowing blood to the overall energy balance, before the critical coagulation temperature.

The heat source  $q$  is induced by the conversion of laser light into heat, the so-called absorbed optical power density, since the heat generated by body metabolism is negligible. The distribution of absorbed energy within the irradiated volume is

TABLE 1. Thermal parameters [21, 24].

	unit	blood	vein wall	perivenous tissue	skin
$k$	$\text{W m}^{-1} \text{ } ^\circ\text{C}^{-1}$	0.52	0.53	0.21	0.21
$\rho$	$\text{kg m}^{-3}$	1060	1080	1000	1109
$c_p$	$\text{J kg}^{-1} \text{ } ^\circ\text{C}^{-1}$	3600	3690	2350	3500
$\omega$	$\text{kg m}^{-3} \text{ s}^{-1}$		1.08	1	0.5545
$A$	$\text{s}^{-1}$	7.6e+66	5.6e+63	5.6e+63	3.1e+98
$E_a$	$\text{J mol}^{-1}$	4.48e+05	4.30e+05	4.30e+05	6.28e+05

governed both by the absorption and the scattering properties of the tissue at the specific wavelength used:

$$q = \mu_a \phi. \quad (5)$$

The heat exchange on the skin surface is given by the Newton law of cooling

$$k \frac{\partial T}{\partial r} + h_{\text{air}}(T - T_{\text{air}}) = 0 \quad \text{if } r = r_s, \quad -vt < z < L, \quad t > 0, \quad (6)$$

where  $h_{\text{air}}$  is the heat transfer coefficient of the air, and  $T_{\text{air}}$  denotes the room temperature. In [21],  $h_{\text{air}}$  is assumed to obey an equation that involves the thermal conductivity of the air, the characteristic length of flow domain, and the Prandtl and Reynolds numbers.

On the remaining boundary, no heat transfer outflow is assumed:

$$\frac{\partial T}{\partial z} = 0 \quad \text{if } 0 < r < r_s, \quad z = -vt, L, \quad t > 0.$$

**2.3. Thermal damage to the vein-tissue system.** Let  $t_{\text{crit}}$  be the time correspondent to the dimensionless indicator of damage when it is equal to one:  $\Omega(t_{\text{crit}}) = 1$ , *i.e.* from the Arrhenius burn integration

$$\frac{1}{A} = \int_0^{t_{\text{crit}}} \exp \left[ -\frac{E_a}{RT(r, z, \tau)} \right] d\tau, \quad (7)$$

where  $R$  is the universal gas constant ( $8.314 \text{ J mol}^{-1} \text{ K}^{-1}$ ),  $A$  is a frequency factor [ $\text{s}^{-1}$ ], and  $E_a$  is the activation energy for the irreversible damage reaction [ $\text{J mol}^{-1}$ ]. Approximating the above integral by the lower and upper Riemann sums with the partition constituted by a finite number  $M$  of subintervals of  $]0, t_{\text{crit}}[$ , of equal length,  $t_{\text{crit}}$  obeys

$$\sum_{m=1}^M \exp \left[ -\frac{E_a}{RT(r, z, mt_{\text{crit}}/M)} \right] < \frac{M}{At_{\text{crit}}} < \sum_{m=1}^M \exp \left[ -\frac{E_a}{RT(r, z, (m-1)t_{\text{crit}}/M)} \right].$$

Thermal damage is consequence of the water content of the constituent cells reaching  $100^\circ\text{C}$ . By this reason, the main predictor of the thermal damage is the dense microbubble formation that is commonly seen at the area.

## 3. AUXILIARY SOLUTIONS

There exist several processes of derivation of the required solutions (see, for instance, [27]). Here, we firstly use the method of separation of variables to find a family of elementary solutions to the parabolic equation and the boundary condition, and then the principle of superposition to construct a solution satisfying the initial condition. Hereafter, the domain subscripts are dropped out by the sake of simplicity whenever the meaning of the parameters is well understood in each domain.

In cylindrical coordinates, the Laplace operator reads (see, for instance, [27, p. 9])

$$\Delta = \frac{\partial^2}{\partial r^2} + \frac{1}{r} \frac{\partial}{\partial r} + \frac{1}{r^2} \frac{\partial^2}{\partial \theta^2} + \frac{\partial^2}{\partial z^2},$$

with  $(r, \theta, z, t) \in ]0; r_o[ \times ]-\pi; \pi[ \times ]0; L[ \times ]0; t_{\text{end}}[$ , where  $r = \sqrt{x^2 + y^2}$  and  $\theta$  is the polar angle measured down from the vertical axis  $z$ .

Taking the angular symmetry, we seek for solutions of the generic PDE:

$$\alpha \frac{\partial v}{\partial t} + b \frac{\partial v}{\partial z} - a \left( \frac{\partial^2 v}{\partial r^2} + \frac{1}{r} \frac{\partial v}{\partial r} + \frac{\partial^2 v}{\partial z^2} \right) + Bv = f, \quad (8)$$

defined in  $]0; r_o[ \times ]0; L[ \times ]0; t_{\text{end}}[$ , with  $v_0$  denoting the initial datum,  $a > 0$ , and  $\alpha, b, B \geq 0$ .

For our purposes, we begin by exemplifying the decomposition followed for the particular function

$$f(r, z, t) = f(t) \chi_{[0; r_f]}(r) \exp[\iota z],$$

where  $\iota \in \mathbb{R}$  and  $\chi_{[0; r_f]}$  stands for the characteristic function over the interval  $[0; r_f]$ .

Thanks to the Duhamel principle, we look for a solution which can be of the form

$$v(r, z, t) = v_2(r, z, t) + \chi_{[0; r_f]}(r) \left( \int_0^t f(s) v_3(r, z, t-s) ds \right) \exp[\iota z], \quad (9)$$

with  $v_2 = C + v_1$ , for some constant  $C$  whenever  $f \equiv BC$ , where  $v_1$  solves (as described in Subsection 3.1)

$$\alpha \frac{\partial v_1}{\partial t} = a \left( \frac{1}{r} \frac{\partial}{\partial r} \left( r \frac{\partial v_1}{\partial r} \right) + \frac{\partial^2 v_1}{\partial z^2} \right) - b \frac{\partial v_1}{\partial z} - Bv_1; \quad (10)$$

$$\frac{\partial v_1}{\partial t}(r, -L, t) = \frac{\partial v_1}{\partial z}(r, L, t) = 0, \quad \forall r, t; \quad (11)$$

$$v_1(r, z, 0) = v_0(r, z), \quad \forall r, z, \quad (12)$$

and  $v_3$  solves

$$\alpha \frac{\partial v_3}{\partial t} + b \frac{\partial v_3}{\partial z} + (B + b\iota - a\iota^2) v_3 = a \left( \frac{1}{r} \frac{\partial}{\partial r} \left( r \frac{\partial v_3}{\partial r} \right) + \frac{\partial^2 v_3}{\partial z^2} \right); \quad (13)$$

$$v_3(r, z, 0) = 1/\alpha, \quad \forall r, z, \quad (14)$$

such that

$$-a \frac{\partial v}{\partial r}(r_s, z, t) + hv(r_s, z, t) = h\gamma, \quad \forall z, t, \quad (15)$$

for some  $\gamma \geq 0$ .

We may consider  $v_3(t) = \exp[\zeta t]/\alpha$  with  $\zeta = (a\iota^2 - b\iota - B)/\alpha$ .

**3.1. Analytical solutions.** Using Bernoulli–Fourier technique, the Cauchy–Robin–Neumann problem admits a solution of the form:

$$v_1(r, z, t) = R(r)Z(z)F(t).$$

In order to obtain an analytical solution, let us take the system of ordinary differential equations (ODE)

$$\begin{cases} F'(t) = \zeta F(t) \\ Z''(z) - (b/a)Z'(z) = \eta^2 Z(z) \\ (rR'(r))' = \beta r R(r), \end{cases} \quad \alpha\zeta = a(\beta + \eta^2) - B. \quad (16)$$

The solution of the first ODE is  $F(t) = A_0 \exp[\zeta t]$ , for some constant  $A_0$ .

The elementary solutions for  $Z$  are

$$\exp \left[ \left( \frac{b}{2a} \pm \Xi \right) z \right],$$

where  $\Xi = (2a)^{-1} \sqrt{b^2 + 4a^2\eta^2}$ .

The elementary solutions for  $R$  are the Bessel functions of first and second kind and order 0, respectively,  $J_0(\sqrt{|\beta|r})$  and  $Y_0(\sqrt{|\beta|r})$  if  $\beta < 0$ ; or the modified Bessel functions of first and second kind and order 0, respectively,  $I_0(\sqrt{\beta r})$  and  $K_0(\sqrt{\beta r})$  if  $\beta > 0$  [27].

We recall their Taylor series expansions around the origin

$$\begin{aligned} J_0(r) &= \sum_{n=0}^{\infty} \frac{(-1)^n}{2^{2n}} \frac{r^{2n}}{n! \Gamma(n+1)}; \\ Y_0(r) &= \frac{2}{\pi} \left( J_0(r) \ln \left[ \frac{r}{2} \right] - \sum_{n=0}^{\infty} (-1)^n \frac{1 + (1/2) + \dots + (1/n) - \gamma}{2^{2n} (n!)^2} r^{2n} \right); \\ I_0(r) &= \sum_{n=0}^{\infty} \frac{1}{2^{2n}} \frac{r^{2n}}{n! \Gamma(n+1)}; \\ K_0(r) &= -I_0(r) \ln \left[ \frac{r}{2} \right] + \sum_{n=0}^{\infty} \frac{1 + (1/2) + \dots + (1/n) - \gamma}{2^{2n} (n!)^2} r^{2n}, \end{aligned}$$

where  $\Gamma$  is the gamma function, and  $\gamma$  is the Euler–Mascheroni constant. Moreover, the following wronskian relationships

$$J_1(\beta r)Y_0(\beta r) - Y_1(\beta r)J_0(\beta r) = \frac{2}{\pi\beta r}; \quad (17)$$

$$K_1(\beta r)I_0(\beta r) + I_1(\beta r)K_0(\beta r) = \frac{1}{\beta r} \quad (18)$$

hold, for any  $\beta > 0$  (see [27, p. 672] and [26, pages 360 and 375]).

Considering  $v_0 = 0$  in  $\Omega_{\text{lumen}}$  and taking  $\beta = -\beta_{1,j}^2$  according to  $j = \text{wall, pad or skin}$ , we find

$$v_1(r, z, t) = 0 \quad \text{in } \Omega_{\text{lumen}}; \quad (19)$$

$$v_1(r, z, t) = A_{1,w} \left( Y_0(\beta_{1,w} r_i) J_0(\beta_{1,w} r) - J_0(\beta_{1,w} r_i) Y_0(\beta_{1,w} r) \right) Z(z) \exp[\zeta t] \quad \text{in } \Omega_w; \quad (20)$$

$$v_1(r, z, t) = \left( A_{1,p} J_0(\beta_{1,p} r) + A_{2,p} Y_0(\beta_{1,p} r) \right) Z(z) \exp[\zeta t] \quad \text{in } \Omega_p; \quad (21)$$

$$v_1(r, z, t) = \left( A_{1,s} J_0(\beta_{1,s} r) + A_{2,s} Y_0(\beta_{1,s} r) \right) Z(z) \exp[\zeta t] \quad \text{in } \Omega_s \quad (22)$$

and the Neumann condition (11) implies that

$$Z(z) = \exp \left[ \frac{b}{2a} z \right] \left( b \sinh [\Xi(L - z)] + \sqrt{b^2 + 4a^2 \eta^2} \cosh [\Xi(L - z)] \right). \quad (23)$$

The above involved constants may be determined by using the continuity conditions on the fluxes and on the functions themselves.

In particular, by the homogeneous Robin condition (15), we have

$$a\beta_{1,s} \left( A_{1,s} J_1(\beta_{1,s} r_s) + A_{2,s} Y_1(\beta_{1,s} r_s) \right) + h \left( A_{1,s} J_0(\beta_{1,s} r_s) + A_{2,s} Y_0(\beta_{1,s} r_s) \right) = 0.$$

Notice that if  $\gamma > 0$  then we have an additional relation, which can be analyzed by adding an additional solution of the form  $R(r) = A_1 I_0(\sqrt{B/ar}) + A_2 K_0(\sqrt{B/ar})$  that obeys

$$-\sqrt{aB} \left( A_1 I_1\left(\sqrt{\frac{B}{a}} r_s\right) - A_2 K_1\left(\sqrt{\frac{B}{a}} r_s\right) \right) + h \left( A_1 I_0\left(\sqrt{\frac{B}{a}} r_s\right) + A_2 K_0\left(\sqrt{\frac{B}{a}} r_s\right) \right) = h\gamma.$$

**3.2. Particular solution.** In this section, we rephrase the particular solution, according to Duhamel principle, in (9)

$$\left( \int_0^t f(s) v_4(r, z, t - s) ds \right) R(r) \exp[\iota z]$$

by taking  $f(r, z, t) = f(t)R(r) \exp[\iota z]$ , where  $\iota \in \mathbb{R}$  and  $R$  denotes any of the Bessel functions of order 0, namely,  $J_0(\sqrt{|\beta|r})$  and  $Y_0(\sqrt{|\beta|r})$  if  $\beta < 0$ ; or the modified Bessel functions of order 0, namely,  $I_0(\sqrt{\beta}r)$  and  $K_0(\sqrt{\beta}r)$  if  $\beta > 0$ , introduced in Subsection 3.1. Analogously, we may consider a solution  $v_4(t) = \exp[\zeta t]/\alpha$  with  $\zeta = (a(\iota^2 + \beta) - b\iota - B)/\alpha$ .

#### 4. RESULTS AND DISCUSSIONS

The primary fluence  $\phi$ , *i.e.* defined in blood whenever the source  $S \neq 0$  (cf. (2)), can be assumed independent on the radius  $r$  as satisfying (8) with  $\alpha = 1/\nu$ ,  $b = 0$ ,  $a = D$ ,  $B = \mu_a$  and  $f = S$ , with  $\iota = -\mu_t$ . Thus, we may choose the particular functions  $v_2 = 0$  and  $v_3(t) = \nu \exp[\zeta t]$ , with

$$\zeta := \nu(D\mu_t^2 - \mu_a) > 0$$

according to Table 2. Then, we have



TABLE 2. Optical parameters [21, 42] (at slow shear rate [36]).

$\lambda$ [nm]	$\mu_a$ [mm <sup>-1</sup> ]				$\mu'_s$ [mm <sup>-1</sup> ]			
	blood	vein wall	tissue pad	skin	blood	vein wall	tissue pad	skin
810	0.21	0.2	0.017	0.2	0.73	2.4	1.2	0.9
980	0.21	0.1	0.03	0.10	0.6	2.0	1.0	0.81
1064	0.12	0.12	0.034	0.10	0.58	1.95	0.98	0.77

$$\phi_\nu(r, z, t) = \frac{\nu S(r_f, z, 0)}{\zeta + \mu_t v} \exp[\zeta t] (1 - \exp[-(\zeta + \mu_t v)t])$$

for  $0 \leq r < r_f$ ,  $-L < z < L$ ,  $0 \leq t < t_{\text{end}}$ . Typically, a laser fiber for medical applications has a 600-micron diameter ( $r_f = 0.3$  mm).

Next, by the interface continuity conditions,  $\phi_\nu$  can be extended as a solution at the position  $(r, z)$  and the time  $t$ ,

$$\begin{aligned} \phi_\nu(r, z, t) &= \frac{\nu S(r_f, z, 0)}{\zeta + \mu_t v} \exp[\zeta t] \\ &\quad + (B_1 J_0(\beta_j r) + B_2 Y_0(\beta_j r)) \exp[-\mu_t(z + vt)] \quad \text{if } r_f < r \leq r_i \quad (j = \text{blood}); \\ \phi_\nu(r, z, t) &= \exp[-\mu_t z] \left( (B_3 I_0(\varkappa_j r) + B_4 K_0(\varkappa_j r)) \exp[\zeta t] \right. \\ &\quad \left. + (B_5 J_0(\beta_j r) + B_6 Y_0(\beta_j r)) \exp[-\mu_t vt] \right) \quad \text{otherwise,} \end{aligned}$$

where the abstract constants  $B_1, \dots, B_6$  are defined by the boundary and interface continuity conditions. The parameters,  $\varkappa_j$  and  $\beta_j$ , are determined due to that the PDE (1) is verified by the function  $\phi$ , namely

$$\begin{aligned} \zeta/\nu_j + \mu_a^{(j)} &= D_j (\mu_t^2 + \varkappa_j^2) \quad j = \text{wall, pad, skin}; \\ -\frac{\mu_t v}{\nu_j} + \mu_a^{(j)} &= D_j (\mu_t^2 - \beta_j^2) \quad j = \text{blood, wall, pad, skin}. \end{aligned}$$

That is,

$$\begin{aligned} \varkappa_j &= \sqrt{\frac{n_{\text{tissue}}}{n_{\text{blood}}} \frac{D \mu_t^2 - \mu_a}{D_j} + (\mu_{\text{eff}}^{(j)})^2 - \mu_t^2} > 0 \quad j = \text{wall, pad, skin}; \\ \beta_j &= \sqrt{\mu_t^2 - (\mu_{\text{eff}}^{(j)})^2 + \frac{\mu_t v}{\nu_j D_j}} > 0 \quad j = \text{blood, wall, pad, skin}. \end{aligned}$$

Here, we may consider  $n = 1.4$  for both the blood and the tissues.

This solution proves that the problem is ill-posed. Although it gives a good answer at the scale of picosecond ( $c = 0.3$  mm ps<sup>-1</sup>), it is inadequate for describing the behavior of the fluence rate whenever the fiber moves. The unsteady  $\phi$  should solves (1) at the

steady state, being such that  $\phi$  attains its maximum at  $z = -vt$ . Then, we have

$$\phi(r, z, t) = B_0 \exp[-\mu_{\text{eff}}(z + vt)] - \frac{S(r_f, 0, 0)}{D\mu_t^2 - \mu_a} \exp[-\mu_t(z + vt)] \quad \text{if } 0 \leq r < r_f; \quad (24)$$

$$\begin{aligned} \phi(r, z, t) = & B_0 \exp[-\mu_{\text{eff}}(z + vt)] \\ & + (B_1 J_0(\beta_b r) + B_2 Y_0(\beta_b r)) \exp[-\mu_t(z + vt)] \quad \text{if } r_f < r \leq r_i; \end{aligned} \quad (25)$$

$$\begin{aligned} \phi(r, z, t) = & (B_3 W_3(\varkappa_{\lambda, j} r) + B_4 W_4(\varkappa_{\lambda, j} r)) \exp[-\mu_{\text{eff}}(z + vt)] \\ & + (B_5 J_0(\beta_j r) + B_6 Y_0(\beta_j r)) \exp[-\mu_t(z + vt)] \quad \text{otherwise,} \end{aligned} \quad (26)$$

where the abstract constants  $B_0, B_1, \dots, B_6$  are defined by the initial, boundary and interface continuity conditions. We consider the modified Bessel functions  $W_3 = I_0$  and  $W_4 = K_0$  if  $\lambda = 810; 1064$  and  $j = \text{wall, skin}$ , or  $\lambda = 980$  and  $j = \text{wall}$ ; and the Bessel functions  $W_3 = J_0$  and  $W_4 = Y_0$  otherwise, in accordance to the factors of the  $r$ -argument

$$\varkappa_{\lambda, j} = \begin{cases} \sqrt{(\mu_{\text{eff}}^{(j)})^2 - \mu_{\text{eff}}^2} > 0 & j = \text{wall, skin;} \\ \sqrt{\mu_{\text{eff}}^2 - (\mu_{\text{eff}}^{(j)})^2} > 0 & j = \text{pad,} \end{cases} \quad \text{if } \lambda = 810; 1064 \quad (27)$$

$$\varkappa_{\lambda, j} = \begin{cases} \sqrt{(\mu_{\text{eff}}^{(j)})^2 - \mu_{\text{eff}}^2} > 0 & j = \text{wall;} \\ \sqrt{\mu_{\text{eff}}^2 - (\mu_{\text{eff}}^{(j)})^2} > 0 & j = \text{pad, skin,} \end{cases} \quad \text{if } \lambda = 980 \quad (28)$$

$$\beta_j = \sqrt{\mu_t^2 - (\mu_{\text{eff}}^{(j)})^2} > 0 \quad j = \text{blood, wall, pad, skin.} \quad (29)$$

Parameters, used in clinical procedures, are known: the power is set at 15 W (with wavelengths of 810 nm and 980 nm) and at 10 W (with wavelengths of 980 nm and 1064 nm). Calculations use Octave software, under the optical parameters in Table 2. Figure 2 (Left) shows the  $\phi$ -profile to the power of 15 W and the wavelength of 810 nm at different instants of time, considering the continuous movement of the fiber tip. The slope decreases from the initial instant of time (solid line)  $z = t = 0$  until the final instant of time (dashed line)  $z = -10, t = 10$ , which reflects the accumulation of the fluence rate. Figure 2 also illustrates the higher distributions only under the tip, as it is experimentally consistent.

As expected, Figure 2 (Right) shows similar profiles between different wavelengths and set powers. At the wavelength of 980 nm, the 15 W-curves (in red) has higher values than the 10 W-curves (in blue). At the power 15 W, the 810 nm-curves (in black) and the 980 nm-curves (in red) match each other, while at the power 10 W, the slope of 980 nm-curves (in blue) is similar than the slope of 1064 nm-curves (in green), but there is no match.

This evaluation improves the study of the absorbed volumetric power  $q$ , and consequently it will improve the study of the distribution of the temperature and make the simulation of the heat transfer closer to reality. Our results are consistent to that the use of laser energies of various wavelengths has no significant difference in their effectiveness and complication rate [22].

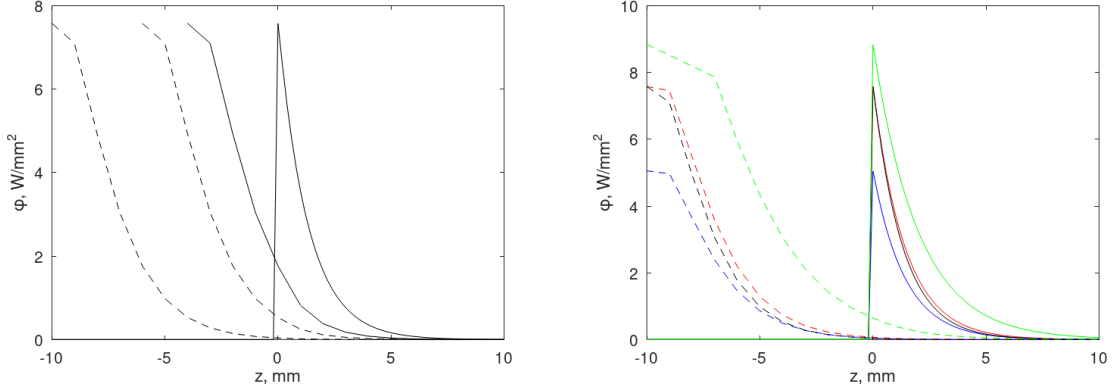


FIGURE 2. Left: Graphical representations of  $\phi$ , at the wavelength of 810 nm, for different instants of time. Right: Graphical representations of  $\phi$  for the wattage set at 15 W: with wavelengths of 810 nm (in black) and 980 nm (in red) and at 10 W: with wavelengths of 980 nm (in blue) and 1064 nm (in green). Solid lines stand for the initial instant of time, while dashed lines stand for the final instant of time.

Hereafter, we assume the solution  $\phi$  as defined by (24)-(29). According to Section 3, let  $T - T_b$  be the thermal solution of (8) with  $\alpha = \rho c_p$ ,  $a = k$ ,  $f = q$ , and

- in the domain  $\Omega_{\text{lumen}}$ :  $b = \rho_b c_b u$  and  $B = 0$ ;
- in the domain  $\Omega_w \cup \Omega_p \cup \Omega_s$ :  $b = 0$  and  $B = c_b \omega$ .

Firstly, at the position  $(r, z) \in [0; r_f[\times] - L; L[$  and the time  $t > 0$ , we split into

- (i):  $f(t) = \mu_a \frac{S(r_f, 0, 0)}{D\mu_t^2 - \mu_a} \exp[-\mu_{\text{eff}}vt]$  and  $\iota = -\mu_{\text{eff}}$ ;
- (ii):  $f(t) = -\mu_a \frac{S(r_f, 0, 0)}{D\mu_t^2 - \mu_a} \exp[-\mu_t vt]$  and  $\iota = -\mu_t$ .

Analogously in the determination of  $\phi_\nu$  we use  $v_3(t) = \exp[\zeta t]/(\rho_b c_b)$  solving (13)-(14) with the factors of the  $t$ - argument

- (i):  $\zeta_1 = k\mu_{\text{eff}}^2/(\rho_b c_b) + u\mu_{\text{eff}}$ .
- (ii):  $\zeta_2 = k\mu_t^2/(\rho_b c_b) + u\mu_t$ .

Secondly, for  $r_f < r < r_i$ , we use  $v_4(t) = \exp[\zeta_3 t]/(\rho_b c_b)$  from Subsection 3.2 with  $\zeta_3 = k\mu_{\text{eff}}^2/(\rho_b c_b) + u\mu_t$  by taking  $\beta_b$  that is given in (29) into account. Next, we

similarly argue for the domain  $\Omega_w \cup \Omega_p \cup \Omega_s$ , concluding

$$T(r, z, t) = T_b + \mu_a B_0 \exp[-\mu_{\text{eff}} z] \frac{\exp[\zeta_1 t] - \exp[-\mu_{\text{eff}} vt]}{k\mu_{\text{eff}}^2 + \rho_b c_b \mu_{\text{eff}}(u + v)} - \frac{\mu_a S(r_f, 0, 0)}{D\mu_t^2 - \mu_a} \exp[-\mu_t z] \frac{\exp[\zeta_2 t] - \exp[-\mu_t vt]}{k\mu_t^2 + \rho_b c_b \mu_t(u + v)} \quad \text{if } 0 \leq r \leq r_f; \quad (30)$$

$$T(r, z, t) = T_b + \mu_a B_0 \frac{\exp[-\mu_{\text{eff}}(z - (k\mu_{\text{eff}}/(\rho_b c_b) + u)t)] - \exp[-\mu_{\text{eff}}(z + vt)]}{k\mu_{\text{eff}}^2 + \rho_b c_b \mu_{\text{eff}}(u + v)} + (B_1 J_0(\beta_b r) + B_2 Y_0(\beta_b r)) \exp[-\mu_t z] \frac{\exp[\zeta_3 t] - \exp[-\mu_t vt]}{k\mu_{\text{eff}}^2 + \rho_b c_b \mu_t(u + v)} + T_1(r, z, t) \quad \text{if } r_f < r \leq r_i; \quad (31)$$

$$T(r, z, t) = T_b + (B_3 W_3(\varkappa_{\lambda, j} r) + B_4 W_4(\varkappa_{\lambda, j} r)) \exp[-\mu_{\text{eff}} z] \times \frac{\exp\left[\sqrt{(k(\mu_{\text{eff}}^{(j)})^2 - \rho_b c_b w)/(\rho c_p)} t\right] - \exp[-\mu_{\text{eff}} vt]}{k(\mu_{\text{eff}}^{(j)})^2 - c_b \omega} + (B_5 J_0(\beta_j r) + B_6 Y_0(\beta_j r)) \exp[-\mu_t z] \times \frac{\exp\left[\sqrt{(k(\mu_{\text{eff}}^{(j)})^2 - \rho_b c_b w)/(\rho c_p)} t\right] - \exp[-\mu_t vt]}{k(\mu_{\text{eff}}^{(j)})^2 - c_b \omega} + T_1(r, z, t) \quad \text{otherwise,} \quad (32)$$

where  $T_1$  is the combination of radial dependent Bessel functions and longitudinal and temporal dependent exponential functions such that (10)-(12) as well as the interface continuity conditions are verified.

As the lumen  $\Omega_{\text{lumen}}$  is constituted by the blood, two different situations exist:

**Case 1.:** The blood flow is obstructed ( $u = 0$ ), for instance the vein is completely clamped or the SSV in the presence of the inserted catheter.

**Case 2.:** The blood flows at  $u = 70 \text{ mm s}^{-1}$ , as such it happens in the GSV. The diameter of the GSV varies from 11 mm to 12 mm at SFJ until 7.5 mm to 8 mm at the proximal thigh (at the knee level) [12].

In the case 1,  $T_1$  is given by (19)-(22) with  $Z(z) = \cosh[\eta(L - z)]$  and

$$\rho_j c_{p, j} \zeta = -k_j(\beta_{1, j}^2 + \eta^2) - c_{p, j} \omega_j \quad j = w, p, s.$$

In the case 2, the solution  $T_1$  depends on the general form (23) of  $Z$ , and (19)-(22) take the dependence on the vein size into account. Known values exist for diameters ranging between 3 and 10 mm, or greater than 10 mm, according to the small saphenous vein (SSV), anterior accessory vein, and great saphenous vein, namely, diameters of 7.5 mm [18],  $r_i = 3.75 \text{ mm}$  and  $\varepsilon = 0.75 \text{ mm}$ , and of 1.2 cm [16],  $r_i = 6 \text{ mm}$  and  $\varepsilon = 1.2 \text{ mm}$ . The proposed solution may address the quantitative questions in the context of the thermal ablation treatment under study. For elucidating the effect of vein diameter, further study will be the aim of future work.

TABLE 3. Upper bounds of  $t_{\text{crit}}$  in seconds.

$^{\circ}\text{C}$	blood	vein wall	perivenous tissue	skin
50	3.4e+05	5.8e+05	5.8e+05	1.1e+03
60	2.3e+03	4.7e+03	4.7e+03	9.5e-01
70	2.1e+01	5.1e+01	5.1e+01	1.3e-03
80	2.4e-01	7.2e-01	7.2e-01	2.5e-06
90	3.6e-03	1.3e-02	1.3e-02	6.9e-09
100	6.8e-05	2.8e-04	2.8e-04	2.6e-11

Finally, we may use the formula (30)-(32) to read the temporal course of damage events from the spatial domain. However, a first analysis should be done. Considering in (7) that  $T \geq T_{\text{min}}$ , we find the following upper bound

$$t_{\text{crit}} \leq \frac{1}{A} \exp \left[ \frac{E_a}{RT_{\text{min}}} \right].$$

Next, if we use the thermal parameters from Table 1, the above upper bound of the critical time  $t_{\text{crit}}$  can be calculated (cf. Table 3) in function of different the minimum surface temperatures. Then, the operating time of 10 s is a safe value for the thermal thresholds for tissue damage at the vein wall, perivenous tissue or skin., the so-called damage temperature ( $T_{\text{min}} = 50^{\circ}\text{C}$ ). This value is consensual among clinicians and researchers in the ablation treatments, [11] and the references therein. We conclude that the interpretation of the vein-tissue system damage substantially disagrees with the critical temperature of  $50^{\circ}\text{C}$  being the temperature that temperatures above it result in necrosis.

The present result shows that the blood coagulates before the dehydration/necrosis of the wall tissue. Moreover, for the blood threshold  $T_{\text{min}} = 100^{\circ}\text{C}$ , the operating time clearly surpasses the upper bound, which is consistent with that a thin layer of carbonized blood is found to cover the fiber tip. Although according to [42] the black layer occurs at temperatures around  $300^{\circ}\text{C}$ . This black layer absorbs an average of 45% of the emitted light power, resulting in a decrease of the tip temperatures.

Indeed, much work remains to be done. The damage of the vein reduces to the vaporisation and occlusion in both above situations, namely cases 1 and 2. The failure and complication rates depend on vein size [7]. Also, the perivenous tumescence injection (tumescence anesthesia) is carried on to protect the perivenous tissue from thermal damage and reduce the lumen of the truncal vein by compression and spasm [38].

## 5. CONCLUSIONS

The derived solutions, namely  $\phi$  and  $T$ , might be a tool to generate quantitative and/or qualitative results. Besides, the configurations of the physical problem solved are questioned. Our main conclusion is that the parabolic equation for the light transport leads to the application of the pulsed laser of the order of picoseconds only, while the elliptic equation leads to the physical solution for a continuous laser light.

## ACKNOWLEDGEMENTS

Deeply thanks to Professor Luís Filipe V. Ferreira by awakening my interest on the light propagation field.

## REFERENCES

- [1] J. Almeida, E. Mackay, J. Javier, J. Mauriello, J. Raines, Saphenous laser ablation at 1470 nm targets the vein wall, not blood, *Vascular and Endovascular Surgery* **43** :5 (2009), 467-472.
- [2] P.R. Anchala, C. Wickman, R. Chen, T. Faundeen, W. Pearce, L. Narducy, S.A. Resnick, Endovenous laser ablation as a treatment for postsurgical recurrent saphenous insufficiency, *Cardiovasc. Intervent. Radiol.* **33** :5 (2010), 983-988.
- [3] J.L. Ash, C.J. Moore, Laser treatment of varicose veins: Order out of chaos, *Seminars In Vascular Surgery* **23** :2 (2010), 101-106.
- [4] L. Bianchi, F. Cavarzan, L. Ciampitti, M. Cremonesi, F. Grilli, P. Saccomandi, Thermophysical and mechanical properties of biological tissues as a function of temperature: a systematic literature review, *International Journal of Hyperthermia* **39** :1 (2022), 297-340.
- [5] A. Caggiati, M. Franceschini, Stroke following endovenous laser treatment of varicose veins, *J. Vasc. Surg.* **51** :1 (2010), 218-220.
- [6] D. Carradice, A.I. Mekako, F.A.K. Mazari, N. Samuel, J. Hatfield, I.C. Chetter, Clinical and technical outcomes from a randomized clinical trial of endovenous laser ablation compared with conventional surgery for great saphenous varicose veins, *Br. J. Surg.* **98** (2011), 1117-1123.
- [7] C.I.O. Chaar, S.A. Hirsch, M.T. Cwenar, R.Y. Rhee, R.A. Chaer, G.A. Hamad, E.D. Dillavou, Expanding the role of endovenous laser therapy: Results in large diameter saphenous, small saphenous, and anterior accessory veins, *Ann. Vasc. Surg.* **25** :5 (2011), 656-661.
- [8] L. Consiglieri, Continuum models for the cooling effect of blood flow on thermal ablation techniques, *Int. J. Thermophys.* **33** :5 (2012), 864-884.
- [9] L. Consiglieri, An analytical solution for a bio-heat transfer problem, *Int. J. Bio-Sci. Bio-Technol.* **5** :5 (2013), 267-278.
- [10] L. Consiglieri, Analytical solutions in the modeling of the local RF ablation, *J. Mech. Med. Biol.* **16** :2 (2016), 1650071 (14 pages).
- [11] L. Consiglieri, I.dos Santos, D. Haemmerich, Theoretical analysis of the heat convection coefficient in large vessels and the significance for thermal ablative therapies, *Phys. Med. Biol.* **48** (2003), 4125-4134.
- [12] S. Doganci, U. Demirkilic, Comparison of 980 nm laser and bare-tip fibre with 1470 nm laser and radial fibre in the treatment of Great Saphenous Vein varicosities: A prospective randomised clinical trial, *Eur. J. Vasc. Endovasc. Surg.* **40** (2010), 254-259.
- [13] O. Etlik, A.A. Korkmaz, Y. Üçkurt, S. Indelen, R. Gündoğdu, A. Öztürk, S. Alsalehi, S.M. Aung, Endovenous laser ablation for saphenous vein insufficiency: long-term results, *Turk. J. Med. Sci.* **43** :3 (2013), 470-473.
- [14] K. Firouznia, H. Ghanaati, M. Hedayati, M. Shakiba, A.H. Jalali, R. Mirsharifi, A. Dargahi, Endovenous laser treatment (EVLT) for the saphenous reflux and varicose veins: A follow-up study, *Journal of Medical Imaging and Radiation Oncology* **57** :1 (2013), 15-20.
- [15] S.S. Gale, J.N. Lee, M.E. Walsh, D.L. Wojnarowski, A.J. Comerota, A randomized, controlled trial of endovenous thermal ablation using the 810-nm wavelength laser and the ClosurePLUS radiofrequency ablation methods for superficial venous insufficiency of the great saphenous vein, *J. Vasc. Surg.* **52** (2010), 645-650.
- [16] M.P. Goldman, M. Mauricio, J. Rao, Intravascular 1320-nm laser closure of the Great Saphenous Vein: A 6- to 12-month follow-up study, *Dermatol. Surg.* **30** (2004), 1380-1385.
- [17] A. González-Suárez, M. Trujillo, F. Burdío, A. Andaluz, E. Berjano, Could the heat sink effect of blood flow inside large vessels protect the vessel wall from thermal damage during RF-assisted surgical resection? *Med. Phys.* **41** :8 (2014), 083301.

- [18] S.D. Goode, A. Chowdhury, M. Crockett, A. Beech, R. Simpson, T. Richards, B.D. Braithwaite, Laser and radiofrequency ablation study (LARA study): A randomised study comparing Radiofrequency Ablation and Endovenous Laser Ablation (810 nm), *Eur. J. Vasc. Endovasc. Surg.* **40** (2010), 246-253.
- [19] T.-L. Horng, W.-L. Lin, C.-T. Liauh, T.-C. Shih, Effects of pulsatile blood flow in large vessels on thermal dose distribution during thermal therapy, *Med. Phys.* **34** :4 (2007), 1312-1320.
- [20] A.N.T.J. Kotte, G.M.J. van Leeuwen and J.J.W. Lagendijk, Modelling the thermal impact of a discrete vessel tree, *Phys. Med. Biol.* **44** (1999), 57-74.
- [21] M.F. Marqa, S. Mordon, E. Hernandez-Osma, M. Trelles, N. Betrouni, Numerical simulation of endovenous laser treatment of the incompetent great saphenous vein with external air cooling, *Lasers Med. Sci.* **28** :3 (2013), 833-844.
- [22] M.E. Memetoğlu, O. Erbasan, D. Özel, Follow-up results of laser saphenous ablation, *Dicle Medical Journal* **39** :3 (2012), 331-335.
- [23] R.J. Min, N. Khilnani, S.E. Zimmet, Endovenous laser treatment of saphenous vein reflux: Long-term results, *J. Vasc. Interv. Radiol.* **14** (2003), 991-996.
- [24] S.R. Mordon, B. Wassmer, J. Zemmouri, Mathematical modeling of endovenous laser treatment (ELT). *BioMed. Eng. OnLine* **5** :26 (2006), 11 pages.
- [25] C.-K. Oh, D.-S. Jung, H.-S. Jang, K.-S. Kwon, Endovenous laser surgery of the incompetent Greater Saphenous Vein with a 980-nm diode laser, *Dermatol. Surg.* **29** (2003), 1135-1140.
- [26] F.W.J. Olver, Bessel functions of integer order, **in** Handbook of mathematical functions with formulas, graphs, and mathematical tables, Chapter 9, pp. 355–389, edited by M. Abramowitz and I.A. Stegun. National Bureau of Standards Applied Mathematics Series 55, United States Department of Commerce, Tenth printing,, Washington, D.C. 1972.
- [27] M.N. Özisik, Heat Conduction. Wiley, New York 1993.
- [28] U. Özkan, Ç. Saritürk, Early clinical improvement in chronic venous insufficiency symptoms after laser ablation of saphenous veins, *Diagn. Interv. Radiol.* **18** :6 (2012), 594-598.
- [29] A.A. Poluektova, W.S.J. Malskat, M.J.C. van Gemert, M.E. Vuylsteke, C.M.A. Bruijninx, H.A.M. Neumann, C.W.M. van der Geld, Some controversies in endovenous laser ablation of varicose veins addressed by optical-thermal mathematical modeling, *Lasers Med. Sci.* **29** (2014), 441-452.
- [30] S.A. Prahl, The diffusion approximation in three dimensions, **in** Optical-thermal response of laser-irradiated tissue, Chapter 7, pp. 207–231, edited by A. J. Welch and M. J. C. van Gemert, Series: Lasers, photonics, and electro-optics, Editor: H. Kogelnik, Springer Science+Business Media, New York 1995.
- [31] E.A. Prince, G.M. Soares, M. Silva, A. Taner, S. Ahn, G.J. Dubel, B.S. Jay, Impact of laser fiber design on outcome of endovenous ablation of lower-extremity varicose veins: results from a single practice, *Cardiovasc. Intervent. Radiol.* **34** :3 (2011), 536-541.
- [32] T. Proebstle, F. Krummenauer, D. Gul, J. Knp, Nonocclusion and early reopening of the great saphenous vein after endovenous laser treatment is fluence dependent, *Dermatol. Surg.* **30** (2004), 174-178.
- [33] A. Puggioni, M. Kalra, M. Carmo, G. Mozes, P. Gloviczki, Endovenous laser therapy and radiofrequency ablation of the great saphenous vein: Analysis of early efficacy and complications, *J. Vasc. Surg.* **42** (2005), 488-493.
- [34] L.H. Rasmussen, M. Lawaetz, L. Bjoern, B. Vennits, A. Blemings, B. Eklof, Randomized clinical trial comparing endovenous laser ablation, radiofrequency ablation, foam sclerotherapy and surgical stripping for great saphenous varicose veins, *Br. J. Surg.* **98** :8 (2011), 1079-1087.
- [35] J. Rathod, K. Taori, M. Joshi, R. Mundhada, A. Rewatkar, S. Dhokane, P. Gour, Outcomes using a 1470-nm laser for symptomatic varicose veins, *J. Vasc. Interv. Radiol.* **21** :12 (2010), 1835-1840.
- [36] A. Roggan, M. Friebel, K. Dörschel, A. Hahn, G. Müller, Optical properties of circulating human blood in the wavelength range 400–2500 nm, *J. Biomed. Opt.* **4** :1 (1999), 36-46.

- [37] M.A. Sharif, C.V. Soong, L.L. Lau, R. Corvan, B. Lee, R.J. Hannon, Endovenous laser treatment for long saphenous vein incompetence, *Br. J. Surg.* **93** :7 (2006), 831-835.
- [38] C.-G. Schmedt, R. Blagova, N. Karimi-Poor, C. Burgmeier, S. Steckmeier, T. Beck, V. Hecht, R. Meier, M. Sadeghi-Azandaryani, B. Steckmeier, R. Sroka, Update of endovenous laser therapy and the latest application studies, *Medical Laser Application* **25** :1 (2010), 34-43.
- [39] T. Schwarz, E. von Hodenberg, C. Furtwangler, A. Rastan, T. Zeller, F.J. Neumann, Endovenous laser ablation of varicose veins with the 1470-nm diode laser, *J. Vasc. Surg.* **51** :6 (2010), 1474-1478.
- [40] W.M. Star, Diffusion theory of light transport, **in** Optical-thermal response of laser-irradiated tissue, Chapter 6, pp. 131–206, edited by A. J. Welch and M. J. C. van Gemert, Series: Lasers, photonics, and electro-optics, Editor: H. Kogelnik, Springer Science+Business Media, New York 1995.
- [41] N.S. Theivacumar, M.J. Gough, Endovenous laser ablation (EVLA) to treat recurrent varicose veins, *Eur. J. Vasc. Endovasc. Surg.* **41** (2011), 691-696.
- [42] P.W.M. van Ruijven, A.A. Poluektova, M.J.C. van Gemert, H.A.M. Neumann, T. Nijsten, C.W.M. van der Geld, Optical-thermal mathematical model for Endovenous Laser Ablation of varicose veins, *Lasers Med. Sci.* **29** (2014), 431-439.
- [43] M.E. Vuylsteke, Th. Martinelli, J. Van Dorpe, J. Roelens, S. Mordon, I. Fourneau, Endovenous Laser Ablation: The role of intraluminal blood, *Eur. J. Vasc. Endovasc. Surg.* **42** (2011), 120-126.

LUISA CONSIGLIERI, INDEPENDENT RESEARCHER PROFESSOR, EUROPEAN UNION

URL: <http://sites.google.com/site/luisaconsiglieri>